Four-wave mixing in three-level systems: Interference and entanglement

Shengwang Du,[1,*] Eun Oh,[2,3] Jianming Wen,[4] and Morton H. Rubin[4]
[1]*Edward L. Ginzton Laboratory, Stanford University, Stanford, California 94305, USA*
[2]*Remote Sensing Division, U. S. Naval Research Laboratory, Washington, D.C. 20375, USA*
[3]*Physics Department, University of Virginia, Charlottesville, Virginia 22904, USA*
[4]*Physics Department, University of Maryland, Baltimore County, Baltimore, Maryland 21250, USA*
(Received 28 February 2007; revised manuscript received 25 April 2007; published 3 July 2007)

The interference of degenerate four-wave mixing (FWM) in three-level systems is examined in both the classical and quantum regimes with a backward configuration. In classical FWM, we find that the phase difference between two indistinguishable FWM transition paths can be varied by different driving laser parameters, and leads to interference in the amplitude and polarization of the generated conjugate field. In the paired-photon generation case, the interference in the nonlinearity disappears because of the time ordering in biphoton generation. However, because of the slow group velocity at the degenerate frequency and polarization, the biphoton-amplitude interference between two Feynman paths can erase the time-ordering information at the detectors. For small group delay, the biphoton correlation, determined by the third-order nonlinearity, shows antibunching and damped Rabi oscillations. For large group delay, where the biphoton bandwidth is determined by phase matching, we show that the biphoton interference leads to a bunching effect. The feasibility of generating polarization entanglement is also discussed.

DOI: 10.1103/PhysRevA.76.013803 PACS number(s): 42.65.Lm, 42.50.Dv, 32.80.−t

Optical four-wave mixing (FWM) has many applications such as phase conjugation [1], real-time holographic imaging [2], and nonlinear frequency conversion [3]. With electromagnetically induced transparency (EIT) [4], FWM has even been demonstrated at low light level [5]. More recently, four-wave spontaneous parametric interactions in cold atomic systems have been used to generate narrowband time-energy entangled photon pairs [6–8].

Earlier work encompassed phase conjugation with degenerate FWM in two-level systems. Du *et al.* [8,9] showed that in a two-level system there is a destructive interference of the third-order nonlinear susceptibility between two FWM processes. Motivated by this work, we study FWM in three-level systems and find that interference, constructive and destructive, of the third-order nonlinear susceptibility of the conjugate field can be realized with different driving laser parameters. In particular, we show that the polarization of the generated conjugate field can also be manipulated. Moreover, the interference of the nonlinearity disappears in the conjugate used to produce entangled photon pairs. However, because the EIT-induced slow-light propagation erases information about time ordering, interference between different two-photon Feynman paths occurs and can modify the correlation from antibunching to bunching. We also discuss generation of paired photons with entangled polarization which has many potential applications, such as tests of Bell's inequalities [10] and quantum-information processing [11]. The paired photons created in such a case are analogous to degenerate type-II spontaneous parametric down-conversion (SPDC) [12,13].

The schematic of FWM in a three-level system is shown in Fig. 1, where pump (ω_p) and coupling (ω_c) lasers counterpropagate through an atomic cloud. A weak probe field (ω_a) is applied to generate its backward phase-matched conjugate field (ω_b). The atomic cloud is in a cigar shape with length L in the probe direction and atomic density N. Two possible FWM transition paths are depicted in Fig. 1(b). The pump and coupling fields have angular frequencies of $\omega_p=\omega_{31}+\Delta_p$ and $\omega_c=\omega_{32}+\Delta_c$, respectively. ω_{31} and ω_{32} are the transition frequencies for $|3\rangle\leftrightarrow|1\rangle$ and $|3\rangle\leftrightarrow|2\rangle$. $\hbar\Delta_{21}$ is the energy difference between two ground levels. The probe frequency is centered at $\varpi_a=\omega_{32}+\Delta_p$, and the conjugate field is centered at $\varpi_b=\omega_{31}+\Delta_c$. If we set $\Delta_p=\Delta_{21}+\Delta_c$, the probe and its conjugate field share the same central frequency, i.e., $\varpi_a=\varpi_b=\omega_0$. We assume that $\Delta_p\gg\Delta_c$ and all the atoms are initially populated in their ground level $|1\rangle$. The third-order nonlinear susceptibilities for two processes can be obtained from perturbation theory [7]:

$$\chi_{\mathrm{I}}^{(3)}(\delta)=\frac{N|\mu_{31}\mu_{32}|^2/(\varepsilon_0\hbar^3)}{(\Delta_{21}+\Delta_c)[|\Omega_c|^2-4(\delta-\Delta_c+i\gamma_{31})(\delta+i\gamma_{21})]}, \tag{1}$$

$$\chi_{\mathrm{II}}^{(3)}(\delta)=\frac{N|\mu_{31}\mu_{32}|^2/(\varepsilon_0\hbar^3)}{(\Delta_{21}+\Delta_c)[|\Omega_c|^2-4(\delta+\Delta_c+i\gamma_{31})(\delta+i\gamma_{21})]}, \tag{2}$$

where $\delta=\omega_a-\omega_0$ is the probe detuning, Ω_c is the coupling Rabi frequency, γ_{ij} are the dephasing rates between levels $|i\rangle$

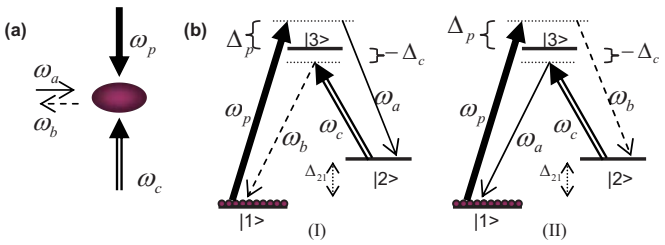

FIG. 1. (Color online) Four-wave mixing in a three-level system. (a) Experimental setup of the right-angle geometry. (b) Two transition paths that produce the ω_b field.

*Electronic address: dus@stanford.edu

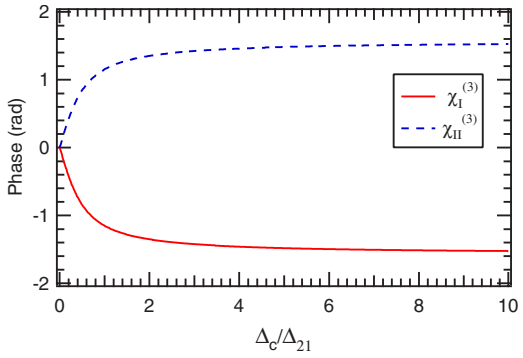

FIG. 2. (Color online) Phases of $\chi_I^{(3)}$ and $\chi_{II}^{(3)}$ vs the normalized coupling detuning Δ_c/Δ_{21}: $\Delta_{21}=2\pi\times 3.036$ GHz, $\gamma_{31}=\gamma_{32}=2\pi\times 3$ MHz, $\gamma_{21}=2\pi\times 0.03$ MHz, $\Omega_c=3\gamma_{31}$, and $\Delta_p=\Delta_{21}+\Delta_c$.

and $|j\rangle$, and μ_{ij} are the dipole matrix elements. One may verify that $\chi_I^{(3)}(\delta)=\chi_{II}^{(3)*}(-\delta)$. The total third-order nonlinear susceptibility is given by $\chi^{(3)}(\delta)=\chi_I^{(3)}(\delta)+\chi_{II}^{(3)}(\delta)$. As seen from Eqs. (1) and (2), at zero coupling detuning ($\Delta_c=0$) the maximum constructive interference occurs, i.e., $\chi_I^{(3)}=\chi_{II}^{(3)}$. For large coupling detuning ($\Delta_c \gg \{\Omega_c, \gamma_{31}, \delta\}$), $\chi_I^{(3)}$ and $\chi_{II}^{(3)}$ have a π phase difference, which indicates a destructive interference with $\chi^{(3)}$. Figure 2 shows the phase of $\chi_{I,II}^{(3)}(\delta=0)$ as a function of coupling detuning. The physics behind this is clear: around $\Delta_c=0$, the nonlinearity is enhanced by the EIT-induced coherence; otherwise, the medium can be approximated as a two-level system [8,9]. To implement the scheme discussed above, the probe field must simultaneously cover both transitions so that interference can occur between the two FWM events and degenerate polarizations.

To study interference between two orthogonal polarizations, we consider the ideal nondegenerate three-state system shown in Fig. 3, where $|1\rangle$, $|2\rangle$, and $|3\rangle$ represent three Zeeman states with $M=-1$, 1, and 0, respectively. The circularly polarized pump and coupling fields are denoted as σ^+ and σ^-. A linearly polarized probe beam, nearly collinear with the pump-coupling direction, can be decomposed into $|\mathcal{P}\rangle_{\text{probe}}=(|\sigma^+\rangle+|\sigma^-\rangle)/\sqrt{2}$. Then the polarization of the ω_b field is $|\mathcal{P}\rangle_{\text{conj}}=(|\sigma^-\rangle+e^{i\phi(\Delta_c)}|\sigma^+\rangle)/\sqrt{2}$ where $\phi(\Delta_c)$ is the phase difference between two FWM events which is determined from $\chi_I^{(3)}$ and $\chi_{II}^{(3)}$. It is obvious that the polarization of the conjugate field depends on Δ_c: (1) for coupling on resonance ($\Delta_c=0$), the conjugate field remains the same linear polarization as the probe because $\phi=0$; (2) for large coupling detuning, $\phi\to\pi$, the conjugate field switches from the horizontal polarization to the orthogonal. Figure 4 shows how the polarization of the conjugate field changes as a function of the coupling detuning with the same parameters used in Fig. 2.

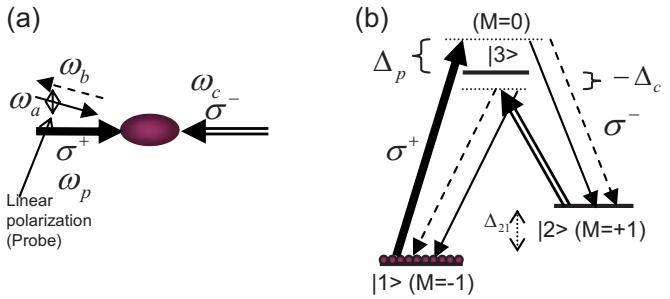

FIG. 3. (Color online) Polarization interference of FWM in an ideal three-state system. (a) Small-angle collinear experimental geometry. (b) Two FWM paths to generate the conjugate field.

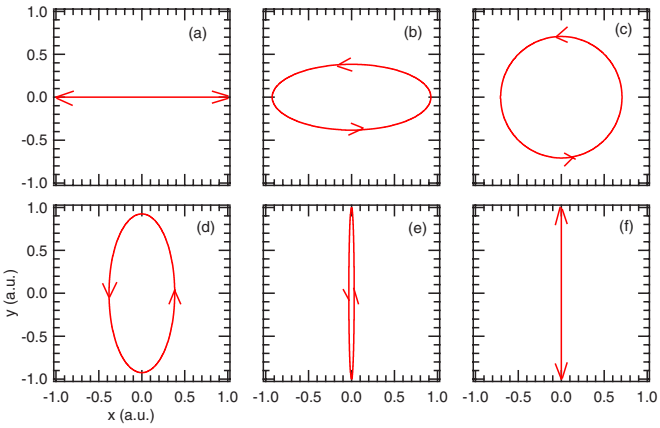

FIG. 4. (Color online) Polarization of the conjugate field generated via the scheme shown in Fig. 3. (a) $\Delta_c=0$, $\phi=0$; (b) $\Delta_c/\Delta_{21}=0.18$, $\phi=\pi/4$; (c) $\Delta_c/\Delta_{21}=0.45$, $\phi=\pi/2$; (d) $\Delta_c/\Delta_{21}=1.08$, $\phi=3\pi/4$; (e) $\Delta_c/\Delta_{21}=14.18$, $\phi=0.98\pi$; (f) $\Delta_c/\Delta_{21}\to\infty$, $\phi=\pi$.

Now we turn to the major part of the two-photon interference when the three-level system is used to generate entangled photon pairs with the same central frequency. As shown in Fig. 5, in the presence of pump and coupling beams, photon pairs are spontaneously emitted into the backward geometry. Here the paired photons are denoted as Stokes (ω_s) and anti-Stokes (ω_{as}). In the following we consider only the case with $\Delta_c=0$ and $\Delta_p=\Delta_{21}$ such that the Stokes and anti-Stokes photons have degenerate spectra. The EIT linear susceptibility is described by

$$\chi(\delta)=\frac{-4N|\mu_{31}|^2(\delta+i\gamma_{21})/(\varepsilon_0\hbar)}{|\Omega_c|^2-4(\delta+i\gamma_{21})(\delta+i\gamma_{31})}. \tag{3}$$

Both Stokes and anti-Stokes photons experience this EIT profile because of their degenerate frequency and polariza-

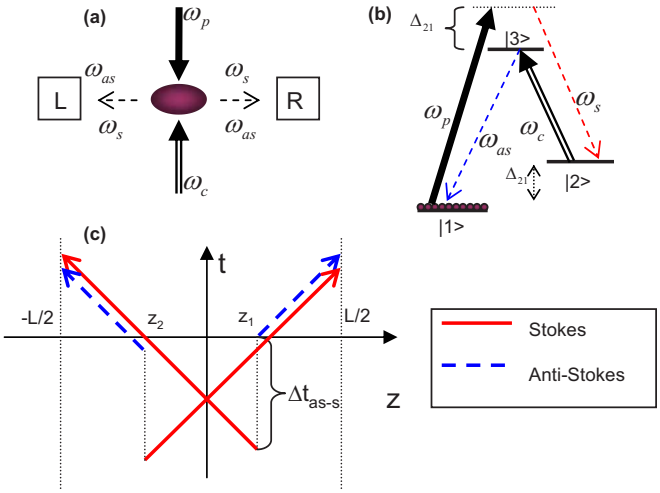

FIG. 5. (Color online) Biphoton generation in a three-level system: (a) Experimental setup; (b) level configuration; (c) Feynman diagram of biphoton interference.

tion. The EIT effect not only prevents the generated photons from being absorbed, but also enhances the nonlinear interaction. As shown in Fig. 5(b), because the Stokes photon is always radiated before the anti-Stokes, there is no interference in the third-order nonlinearity. However, because both Stokes and anti-Stokes photons experience slow group velocity, their time-ordering information is washed out when the group delay is larger than the generation time, i.e., $L/V_g \geqslant \Delta t_{as\text{-}s}$. This may be understood with the help of the Feynman diagram in Fig. 5(c). We are interested in the case that two detectors tend to fire simultaneously by postselection. Since the anti-Stokes photon is emitted after the Stokes, by adjusting the coincidence window paired Stokes–anti-Stokes photons are considered if they are registered almost at the same time by the two detectors. Two possible Feynman paths for such a measurement are shown in Fig. 5(c). Regardless of where the pair is generated, z_1 or z_2, they are not distinguished by the detectors. Hence the interference occurs between two different Feynman paths.

The two-photon amplitude in the time domain on the output surfaces is

$$\Psi(t_L,t_R) = \Psi_{s\text{-}as}(t_L,t_R) + \Psi_{s\text{-}as}(t_R,t_L), \tag{4}$$

where R and L refer to right- and left-propagating modes. The paired Stokes–anti-Stokes amplitude can be obtained using perturbation theory [13,14]:

$$\Psi_{s\text{-}as}(\tau) = \frac{L}{2\pi}\int d\delta\, \kappa(\delta) e^{i(k_s+k_{as})L/2}\Phi(\Delta kL)e^{-i\delta\tau} \tag{5}$$

where $\tau=t_{as}-t_s$ is the time delay between the two detectors, $\kappa(\delta)=(i\omega_0/2c)\chi_1^{(3)}(\delta)E_pE_c$ is the nonlinear coupling coefficient, and $\Delta k=k_s-k_{as}$ is the phase mismatching inside the medium and is approximated as $\Delta k=2\delta/V_g$. The term $e^{i(k_s+k_{as})L/2}$ can be removed because $k_s+k_{as}=2k_0$ is a constant. The longitudinal detuning function is defined as

$$\Phi(\Delta kL) = \frac{1}{L}\int_{-L/2}^{L/2} dz\, e^{-i\Delta kz} \simeq \mathrm{sinc}\left(\frac{\delta L}{V_g}\right), \tag{6}$$

which allows Eq. (5) to be expressed as a convolution:

$$\Psi_{s\text{-}as}(\tau) = \Psi_0(\tau) * \Pi(\tau), \tag{7}$$

with

$$\Psi_0(\tau) = \frac{L}{2\pi}\int d\delta\, \kappa(\delta)e^{-i\delta\tau} = Be^{-\gamma_e\tau}\sin\left(\frac{\Omega_e\tau}{2}\right)\theta(\tau), \tag{8}$$

where $\gamma_e=(\gamma_{21}+\gamma_{31})/2$ and $\Omega_e=\sqrt{\Omega_c^2-(\gamma_{21}-\gamma_{31})^2}$. B is a constant. The rectangular function $\Pi(\tau)=V_g/(2L)$ for $\tau \in [-L/V_g, L/V_g]$, and otherwise zero, is a Fourier transform of the longitudinal function. The Heaviside function $\theta(\tau)$ defines $\Psi_0(\tau)$ as valid for $\tau \geqslant 0$. Now the biphoton amplitude [Eq. (4)] becomes

$$\Psi(\tau = t_R - t_L) = [\Psi_0(\tau) + \Psi_0(-\tau)] * \Pi(\tau). \tag{9}$$

As shown, even though there is no temporal overlapping between $\Psi_0(\tau)$ and $\Psi_0(-\tau)$, their convolution with $\Pi(\tau)$ will mix them together. Two characteristic times of the system are the group delay $\tau_g=L/V_g$ and the Rabi oscillation period $\tau_r=2\pi/\Omega_e$. When $\tau_g \ll \tau_r$, we can treat $\Pi(\tau)$ as a delta function $\delta(\tau)$ and approximate $\Psi(\tau)$ as $\Psi_0(\tau)+\Psi_0(-\tau)$. For this case, interference is not present between $\Psi_0(\tau)$ and $\Psi_0(-\tau)$ and photon antibunching at $\tau=0$ is observed where the two-photon correlation exhibits a damped Rabi oscillation. If $\tau_g \gg \tau_r$, however, the two-photon temporal correlation approaches a rectangularlike function [i.e., $\Psi(\tau)\rightarrow\Pi(\tau)$] and exhibits photon bunching around $\tau=0$.

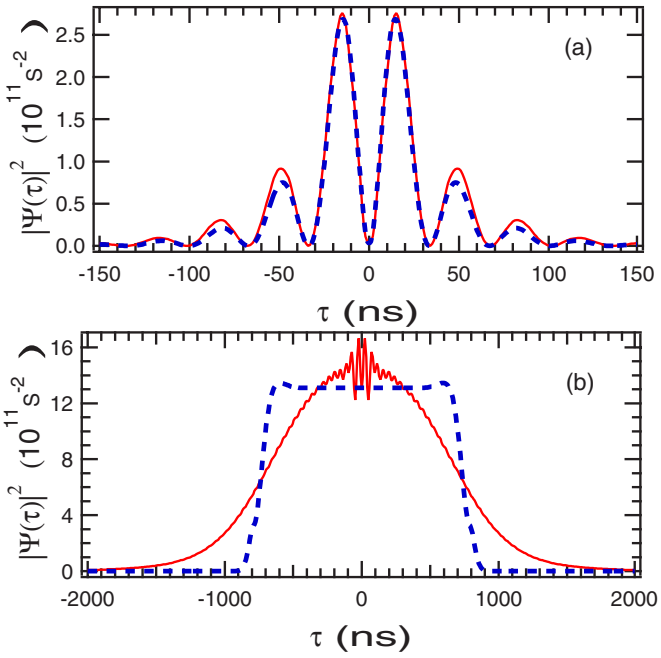

FIG. 6. (Color online) Two-photon correlation $|\Psi(\tau)|^2$ as a function of time delay τ. The blue dashed line represents the results from the perturbation theory and the red solid line stands for those from the Maxwell coupled operator equations. (a) Small-group-delay regime: OD=1.5, $\Omega_c=10\gamma_{31}$, $\tau_g=1.6$ ns, and $t_r=33.5$ ns; (b) large-group-delay regime: OD=30, $\Omega_c=2\gamma_{31}$, $\tau_g=788$ ns, and $t_r=193$ ns.

The numerical simulations (blue dashed line) are given in Fig. 6, where a comparison is made with the methodology by solving the coupled operator equations [6–8] which include both the linear loss and Raman gain profiles (red solid line). We have chosen the ^{85}Rb $D2$ line for a suitable level configuration: $|1\rangle=|5S_{1/2},F=2\rangle$, $|2\rangle=|5S_{1/2},F=3\rangle$, $|3\rangle=|5P_{3/2},F=3\rangle$, $\Delta_{21}=2\pi\times 3.036$ GHz, $\gamma_{31}=\gamma_{32}=2\pi\times 3$ MHz, $\gamma_{21}=2\pi\times 0.03$ MHz, and $\Omega_p=100\gamma_{31}$. The cold atomic cloud, prepared in a two-dimensional magneto-optical trap, has a typical longitudinal length of 1.5 cm and an optical depth (OD) of 30 at the pump transition [15]. For small group delay with low OD ($\sim$1.5) and large coupling Rabi frequency ($\Omega_c=10\gamma_{31}$), two methods yield the same result. As seen in Fig. 6(a), the two-photon correlation shows a damped Rabi oscillation and photon antibunching. For large group delay with high OD ($\sim$30) and small coupling Rabi frequency ($\Omega_c=2\gamma_{31}$), as shown in Fig. 6(b), perturbation theory [Eq. (9)] shows that the correlation becomes a rectangularlike shape and the coincidences at $\tau=0$ are not zero. The coupled operator equations predict similar behavior except that the loss and gain modify the pattern.

We note that the three-state scheme (Fig. 3) can also be used to generate polarization-entangled paired photons. The polarization-entangled state takes the form [16]

$$|\Psi\rangle = \Psi_{s\text{-}as}(\tau)|\sigma^+,\sigma^-\rangle + \Psi_{s\text{-}as}(-\tau)|\sigma^-,\sigma^+\rangle. \quad (10)$$

Maximum polarization entanglement can be achieved if the generation time difference is compensated. Again, there is no interference between two orthogonal circular polarizations in a single-photon counting experiment because the reduced density operator for a single photon is always $\hat{\rho}=(|\sigma^+\rangle\langle\sigma^+| + |\sigma^-\rangle\langle\sigma^-|)/2$. The reason is that when twin photons are generated in a single event following a time ordering of atomic transitions, each photon can occupy only one transition due to the polarization and time-energy entanglement. There is no interference between different events because of the random nature of spontaneous emission. For application purposes, the polarization-entangled Stokes and anti-Stokes photons have long coherence length and coherence time, which is ideal for long-distance quantum communication.

In summary, we have studied interference of classical FWM and biphoton generation in three-level systems with a back-to-back configuration. In classical FWM, we find that the phase difference between two FWM transition paths can be varied by adjusting the input laser parameters. In a three-state scheme, we show that the polarization of the conjugate field can be manipulated. In the paired-photon generation scheme, the interference in the nonlinearity disappears because of the time ordering in the generation mechanism. However, the EIT-induced slow-light propagation is experienced by both Stokes and anti-Stokes photons because of their degenerate frequency and polarization, and acts as a quantum eraser of the time ordering. An interference appears as a sum of indistinguishable biphoton amplitudes from different Feynman paths. For small group delay, the biphoton temporal correlation is mainly determined by the third-order nonlinearity and exhibits photon antibunching and damped Rabi oscillations. For large group delay, the biphoton bandwidth is determined by phase matching and the two-photon interference yields photon bunching. Generating polarization entanglement is also suggested in the three-state case, which is similar to type-II SPDC. We also emphasize that the nonlinear coupling coefficients for the classical FWM coupled field equations are different from those used in coupled operator equations. In general, considering biphoton generation in the schemes proposed in this paper, it is not valid to directly change the classical FWM coupled field equations into operator equations (e.g., [5–7]) without changing the nonlinear coupling coefficients.

S.D. was supported by the Defense Advanced Research Projects Agency, the U.S. Air Force Office of Scientific Research, and the U.S. Army Research Office. E.O. was supported in part by the Office of Naval Research. J.-M.W. and M.H.R. were supported in part by the U.S. ARO MURI Grant No. W911NF-05-1-0197.

[1] R. W. Hellwarth, J. Opt. Soc. Am. **67**, 1 (1977); T. Fu and M. Sargent III, Opt. Lett. **5**, 433 (1980).
[2] H. J. Gerritsen, Appl. Phys. Lett. **10**, 239 (1967); A. Yariv, IEEE J. Quantum Electron. **QE-14**, 650 (1978).
[3] A. J. Merriam, S. J. Sharpe, M. Shverdin, D. Manuszak, G. Y. Yin, and S. E. Harris, Phys. Rev. Lett. **84**, 5308 (2000).
[4] S. E. Harris, Phys. Today **50**(7), 36 (1997).
[5] D. A. Braje, V. Balic, S. Goda, G. Y. Yin, and S. E. Harris, Phys. Rev. Lett. **93**, 183601 (2004).
[6] V. Balić, D. A. Braje, P. Kolchin, G. Y. Yin, and S. E. Harris, Phys. Rev. Lett. **94**, 183601 (2005).
[7] P. Kolchin, S. Du, C. Belthangady, G. Y. Yin, and S. E. Harris, Phys. Rev. Lett. **97**, 113602 (2006).
[8] S. Du, J.-M. Wen, M. H. Rubin, and G. Y. Yin, Phys. Rev. Lett. **98**, 053601 (2007).
[9] J.-M. Wen, S. Du, and M. H. Rubin, Phys. Rev. A **75**, 033809 (2007).
[10] J. S. Bell, Physics (Long Island City, N.Y.) **1**, 195 (1964).
[11] N. Gisin *et al.*, Rev. Mod. Phys. **74**, 145 (2002).
[12] P. G. Kwiat, K. Mattle, H. Weinfurter, A. Zeilinger, A. V. Sergienko, and Y. Shih, Phys. Rev. Lett. **75**, 4337 (1995).
[13] M. H. Rubin, D. N. Klyshko, Y. H. Shih, and A. V. Sergienko, Phys. Rev. A **50**, 5122 (1994).
[14] J.-M. Wen and M. H. Rubin, Phys. Rev. A **74**, 023808 (2006).
[15] M. Vengalattore and M. Prentiss, Phys. Rev. Lett. **95**, 243601 (2005).
[16] J.-M. Wen, S. Du, and M. H. Rubin (unpublished).